Earthquakes and Structures, *Vol. 15, No. 2 (2018) 123-132*
DOI: https://doi.org/10.12989/eas.2018.15.2.123

Criterion for judging seismic failure of suspen-domes based on strain energy density

Ming Zhang[*1], Gerry Parke[2], Shixuan Tian[3a], Yanxia Huang[**1] and Guangchun Zhou[4b]

[1]*School of Civil Engineering, Southwest Jiaotong University, Chengdu 610031, China*
[2]*Department of Civil and Environmental Engineering, University of Surrey, Guildford GU2 7XH, UK*
[3]*Beijing Branch, Arup International Consultant (Shanghai) Co. Ltd, Beijing, China*
[4]*School of Civil Engineering, Harbin Institute of Technology, 73 Huang he Road, Harbin, China*

(Received December 10, 2017, Revised January 28, 2018, Accepted April 18, 2018)

Abstract. In this paper the strain energy density (SED) model is used to analyze the seismic behavior of suspen-domes and a new criterion is established for judging the seismic failure based on a characteristic point in the SED model. Firstly, a nonlinear time-history response analysis was carried out using the finite-element package ANSYS for typical suspen-domes subjected to different ground motions. The seismic responses including nodal displacements, ratios of yielding members, strain energy density and structural maximum deformation energy were extracted corresponding to the increasing peak ground acceleration (A). Secondly, the SED sum (I_d) was calculated which revealed that the I_d -A curve exhibited a relatively large change (called a characteristic point) at a certain value of A with a very small load increment after the structures entered the elastic-plastic state. Thirdly, a SED criterion is proposed to judge the seismic failure load based on the characteristic point. Subsequently, the case study verifies the characteristic point and the proposed SED criterion. Finally, this paper describes the unity and application of the SED criterion. The SED method may open a new way for structural appraisal and the SED criterion might give a unified criterion for predicting the failure loads of various structures subjected to dynamic loads.

Keywords: suspen-dome; SED criterion; characteristic point; failure load; nonlinear time-history response analysis

1. Introduction

The suspen-dome is a new style of space structure, which is formed by combining a single-layer reticulated shell and a cable-strut system (Chen *et al*. 2016). Compared with traditional single-layer reticulated shell structures, suspen-domes exhibit a more uniform spatial stiffness distribution, have less thrust on supports, and consequently show a stronger spanning capacity (Zhou *et al*. 2014).

Most current research on suspen-domes focus on dynamic analyses including natural vibration and seismic response analysis, static analysis, which partly consists of linear, nonlinear buckling analysis and the influence of boundary conditions (Chen *et al*. 2016, Chen *et al*. 2010, Chen *et al*. 2010, Guo 2011, Guo *et al*. 2012, Chen and Feng 2015). Also other key factors affect the structural performance of these structures such as the design of the pre-stresses for the cables, sliding control between cables and pulleys or the hoop cable around a cable joint and the influence of joint stiffness (Chen *et al*. 2016, Gao and Weng 2004, Kitipornchai *et al*. 2005, Chen *et al*. 2011, Liu and Chen 2012, Chen *et al*. 2015). Research has also been presented on the structural design (Kang *et al*. 2003, Zhang *et al*. 2009, Zhang *et al*. 2011) of these interesting structures including construction simulation analysis (Li *et al*. 2012, Chen *et al*. 2015) and structural optimization (Liu *et al*. 2016) based on both experimental and numerical simulations. Unfortunately, the seismic failure analysis, particularly the failure of structures under a strong earthquake, has not been adequately investigated. For structural failure, existing research is concentrated on the dynamic failure criteria of single-layer lattice shells rather than on suspen-domes (Shen *et al*. 2005, Zhi *et al*. 2010).

It is well known that earthquakes occur frequently, such as the Wenchuan Earthquake (Ms 8.0) and the Haiti Earthquake (Ms 7.0), Chile Earthquake (Ms 8.2), East Japan Earthquake (Ms 9.0), and so on. These earthquakes seriously threaten the safety of suspen-domes and cause structural problems which may result in failure in turn affecting human lives and property. Therefore, there is an urgent need to establish a criterion to predict, as accurately as possible, the failure load to permit the design and construction of reliable and economic suspen-domes which can provide large and safe spaces for people, especially during a massive earthquake.

In view of the above issues, this paper develops a novel model for investigating seismic behavior of suspen-domes based on strain energy density (SED). Initially, the suspen-dome model is introduced, followed by the analysis method adopted in the finite element package ANSYS (ANSYS 10.0 2005) as well as the structural classification. The nonlinear time-history response analysis for typical suspen-

*Corresponding author, Ph.D.
E-mail: huangyx@home.swjtu.edu.cn
**Corresponding author, Ph.D.
E-mail: zhangming@home.swjtu.edu.cn
[a]Assistant Engineer
[b]Professor

http://www.techno-press.com/journals/eas&subpage=7
ISSN: 2092-7614 (Print), 2092-7622 (Online)

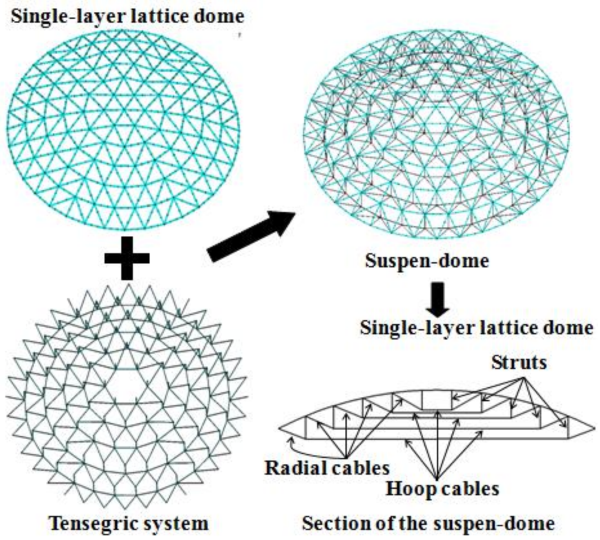

Fig. 1 The suspen-dome

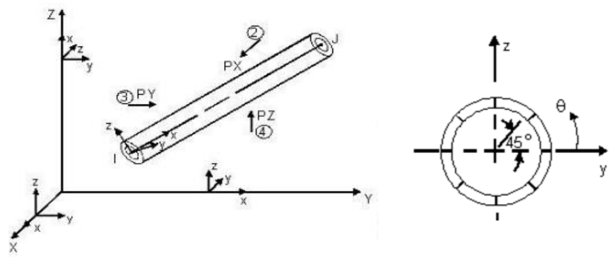

Fig. 2 The PIPE20 geometry (ANSYS 10.0 2005)

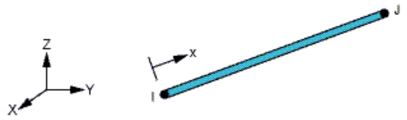

Fig. 3 The LINK8 geometry (ANSYS 10.0 2005)

domes subjected to harmonic actions and different seismic actions, is investigated with different failure modes and the numerical results are discussed. This lays the foundations for the new model, namely, the relationship between the sum of the SED (I_d) and the peak ground acceleration (A). Thirdly, the proposed SED criterion based on the revealed characteristic point in the I_d-A curves is highlighted followed by the verification of the SED criterion using typical case studies. Fourthly, the unity of the SED criterion for strength failure and dynamic instability is presented. Last but not least, guidance on the design process using the SED criterion referring to the Chinese design code is presented (Chinese Standard 2010).

2. The suspen-dome model

The suspen-dome (Kang *et al*. 2003, Chen *et al*. 2010), as shown in Fig. 1, is constructed from a single-layer lattice dome, struts and radial and hoop cables with the appropriate pre-stresses. The ends of the struts hanging from the same ring of joints of the single-layer lattice dome are connected with the next ring of joints by radial cables, which are connected with each other by hoop cables, as the section of the suspen-dome shows. Struts, radial and hoop cables, form a tensegric system which sustains vertical loads together with the single-layer lattice dome and, therefore, provide a more efficient and economic way of constructing large-span domes.

A nonlinear full-range analysis was carried out for each scaled peak ground acceleration using the finite-element package ANSYS, with all the supports of the suspen-dome models fixed against translation but free for rotation; the joints between the members were taken as rigid. The roof weight was 1 kN/m^2 and the nodal load was equivalent to the surface area supported and the lumped masses applied to the nodes are described by the point elements MASS21 (ANSYS 10.0 2005). Both geometrical and material nonlinearities were considered in the dynamic analysis (Li *et al*. 2003). From the innermost ring to the outermost ring of the suspen-dome, the cable prestress forces of the hoop cables are 5 kN, 10 kN, 20 kN, 50 kN and 100 kN respectively. The PIPE20 (ANSYS 10.0 2005) beam element was selected to simulate the members of the single-layer lattice dome; the LINK8 (ANSYS 10.0 2005) and the LINK10 (ANSYS 10.0 2005) elements were used to model the struts and cables respectively. The bilinear isotropic hardening model for all elements was adopted. The numerical model used a yield stress of 345 MPa and a Young's modulus E of 2.06×10^5 MPa for the PIPE20 and LINK8 elements; a yield stress of 1330 MPa and a Young's modulus E of 1.8×10^5 MPa were used for the LINK10 cable elements. Rayleigh damping was assumed based on the natural periods of the first and second modes, and the damping ratio was assumed to be 0.02.

The PIPE20 (ANSYS 10.0 2005) element is a uniaxial element with tension-compression, bending, and torsion capabilities as shown in Fig. 2. The element has six degrees of freedom at each node: translations in the nodal, x, y, and z directions, and rotations about the nodal x, y, and z axes. The element has plastic, creep and swelling capabilities, and it can output nodal displacements, member forces for nodes, axial stress, maximum bending stress at the outer surface, shear strains, strain energy, and so on. In addition, there were eight integration points distributing uniformly around the cross-section of the PIPE20, which can output all the data mentioned above.

The LINK8 element (ANSYS 10.0 2005) is a spar which may be used in a variety of engineering applications as shown in Fig. 3. This element can be used to model trusses, sagging cables, links, springs, etc. The 3-D spar element is a uniaxial tension-compression element with three degrees of freedom at each node: translation in the nodal x, y, and z directions. As in a pin-jointed structure, no bending of the element is considered.

Similar to LINK8, LINK10 (ANSYS 10.0 2005) is also a 3-D spar element. But it has the unique feature of a bilinear stiffness matrix resulting in a uniaxial tension-only (or compression-only) element. With the tension-only option, the stiffness is removed if the element goes into compression (simulating a slack cable of slack chain condition). The element can output nodal displacements, axial stress, strain, and so on.

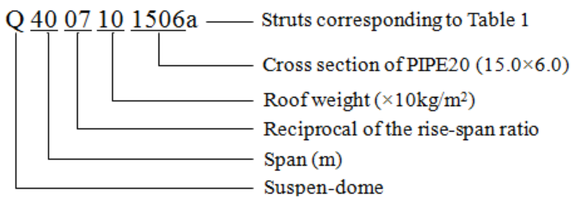

Fig. 4 Classification of the suspen-domes

Table 1 The heights of the struts

Span (m)	Position	*a* (m)	*b* (m)	*c* (m)	*d* (m)	*e* (m)	*f* (m)
40	The three inner rings	2.0	2.4	2.4			
	The two outer rings	3.0	3.5	3.2			
60	The four inner rings				2.8	3.2	3.6
	The three outer rings				4.2	4.0	4.5

Table 2 The cross section of the cables

Span of the suspen-dome (m)	Hoop	Cross section of hoop cables (mm^2)	Cross section of radial cables (mm^2)
40	1	84.8	236
	2	236	
	3	285	
	4	462	
	5	851	
60	1	84.8	236
	2	191	
	3	236	
	4	285	
	5	339	
	6	530	
	7	851	

The classification of the suspen-domes with the different heights of the struts and cross sections of the cables are listed in Tables 1 and 2 as well as other information which is shown in Fig. 4.

3. The failure modes extracted using ANSYS

3.1 Responses of suspen-domes under harmonic actions

Harmonic actions are the most basic dynamic loads, and the study of the suspen-dome under harmonic actions with different frequencies can reveal the essential effects of the spectral characteristics of a dynamic load on the responses of the suspen-domes (Zhi *et al*. 2007). Therefore, the normalize spectra for suspen-domes are conducted to select a typical harmonic action, taking the linear harmonic response spectrum of dome Q4007101506a under horizontal and vertical harmonic actions for example, as shown in Fig. 5.

In order to investigate the different structural performance, the harmonic wave with a frequency 5 Hz was used as the input ground motion, the frequency falls in the resonant zone for most suspen-domes, but not for all structural types. The seismic responses of the suspen-domes

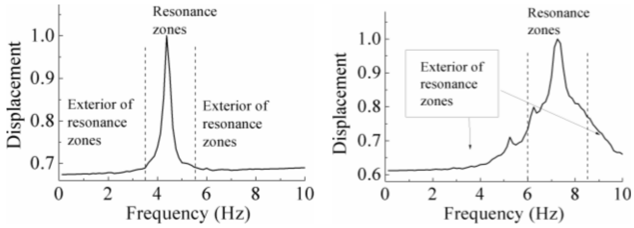

(a) Horizontal (b) Vertical

Fig. 5 Linear harmonic response spectrum

under harmonic wave with a frequency 5 Hz not only represent the resonant response for some suspen-domes, but also embody the nonresonant response for some suspen-domes. Hence, the analysis results can represent the seismic responses of suspen-domes under harmonic actions.

Under the harmonic action with a frequency 5 Hz, some responses of suspen-domes were selected to evaluate their seismic behavior mainly through the relationship between these structural responses and load intensity *A*. These representative responses are defined as follows (Zhi *et al*. 2010):

(1) The ratio of members with different levels of the development in plastic deformation $R_{n\mathrm{P}}$ on the cross-section, is shown in Fig. 6(a). There were eight integration points used for each cross-section. The symbol *n*P indicates that there are *n* integration points on the cross-section which have yielded, thus 8P indicates that the whole cross-section has yielded. Here the ratio of *n*P is the percentage of the members whose yield levels are greater than or equal to an *n*P member. The ratios of yielding members represent the range and the level of plastic yielding, in other words, the higher the ratio of yielding members, the more extensive the development of structural plastic deformation. The following gives a short explanation of the key parameters used in the investigation.

(2) The maximum displacement (*D*) is the maximum deformation value in a suspen-dome throughout the whole dynamic process.

(3) The structural maximum deformation energy (SMDE) is the maximum deformation energy in a suspen-dome throughout the whole dynamic process.

(4) The contours of displacement are the lines of equal nodal displacement in a suspen-dome.

(5) The structural yield point is when the elements of the structure yield. The structure is considered to be in the elastic-plastic range, and the foremost point of the elastic-plastic range is defined as the structural yield point.

(6) The yield load is the load corresponding to the structural yield point.

Based on the above definitions the seismic responses for Q4007101506a subjected to a 3-D harmonic action are shown in Fig. 6. As shown in Fig. 6(a), when the load peak ground acceleration exceeds 3.00 m/s^2, the suspen-dome begins to yield ($R_{1\mathrm{P}}$ is more than 0). Also when the peak ground acceleration *A* reaches 4.00 m/s^2, the $R_{8\mathrm{P}}$ is greater than 0, namely, the yield of the entire sections occurs for some members. Then, the $R_{n\mathrm{P}}$ increases steadily with the increase of *A*, which means that the increasing dynamic load gradually deepens the structural yield level. Similar to

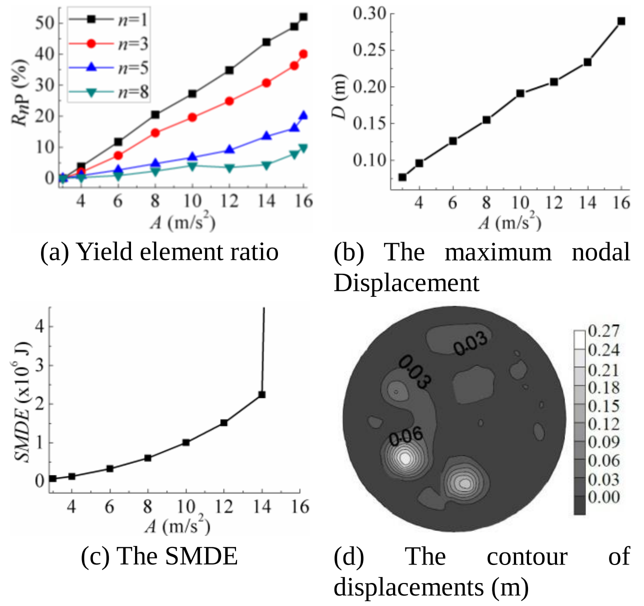

(a) Yield element ratio (b) The maximum nodal Displacement

(c) The SMDE (d) The contour of displacements (m)

Fig. 6 The dynamic full-range analysis of suspen-dome Q4007101506a under horizontal harmonic actions (5 Hz)

Table 3 Structural responses of different suspen-domes subjected to 3-D harmonic action (5 Hz)

Label of suspen-domes	Yield load* (m/s²)	Failure load* (m/s²)	Characteristic responses			
			D (m)	SMDE ($\times 10^6$ J)	R_{1P} (%)	R_{8P} (%)
Q4007101506a	3.25	14.00	0.23	2.24	43.86	4.39
Q4008101506a	7.00	16.50	0.32	3.51	49.72	12.61
Q4007121506a	5.00	18.00	0.27	6.63	65.79	14.03
Q4010121806b	8.75	12.50	0.12	0.29	9.65	1.46
Q4010081606c	7.00	18.00	0.25	1.15	30.11	3.80
Q6007082008d	8.25	13.00	0.19	1.85	16.83	2.00
Q6007102008d	8.00	10.40	0.11	0.35	2.16	0.17
Q6010102510e	4.80	12.31	0.23	3.53	21.16	0.83

* Peak Ground Acceleration (m/s²)

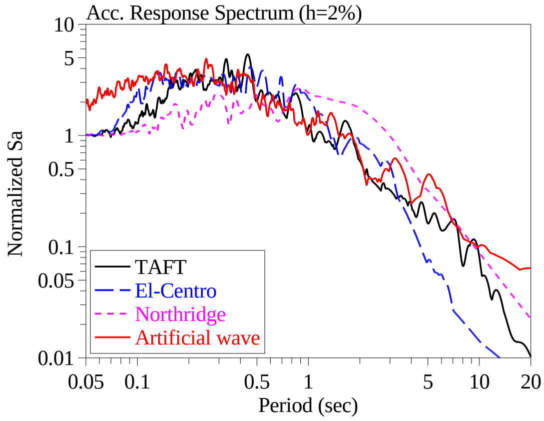

Fig. 7 Spectrum characteristics of earthquakes

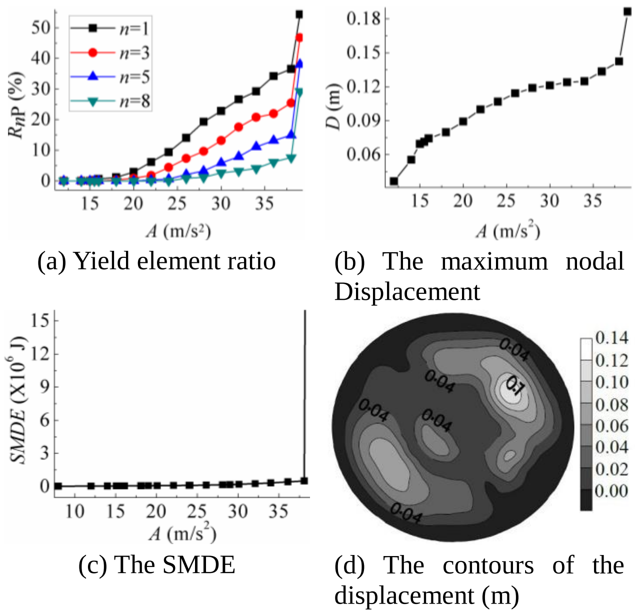

(a) Yield element ratio (b) The maximum nodal Displacement

(c) The SMDE (d) The contours of the displacement (m)

Fig. 8 The dynamic full-range analysis of Q4007101506a under the Taft wave

the R_{nP}, the maximum displacement D also increases linearly with the increase in A as shown in Fig. 6(b). From Figs. 6(a) and (b), it can be judged that the suspen-dome has exceeded its serviceability limit state before the peak ground acceleration of 16.00 m/s² has been reached due to extensive plastic deformation (Shen *et al*. 2005, Zhi *et al*. 2010, Zhi *et al*. 2007) and large displacement occurring (Chinese Standard 2010). However, it is not possible to calculate the accurate failure load of the suspen-dome theoretically. Fortunately, the SMDE increases dramatically at 14m/s² after a relatively stable increase following the increasing in A as shown in Fig. 6(c), which means that the structural normal working state has changed when the load amplitude peaks at 14.00 m/s². Considering Fig. 6(a), (b) and (c), the value of A=14.00 m/s² is defined as the failure load of the suspen-dome. Furthermore, the local and global deformation can be checked roughly by scanning the contour of displacement corresponding to the failure load as shown in Fig. 6(d). For suspen-dome Q4007101506a, the most severe deformation appears in the lower part of the structure.

The results for the selected suspen-domes subjected to the same harmonic action are listed in the Table 3.

From Table 3, it can been seen that the suspen-domes Q4007101506a, Q4008101506a, Q4007121506a, S4010081606c and Q6010102510e display extensive development of plastic deformation and large displacements before collapse, which are approaching the dynamic strength failure based on Chen *et al*. (2011). The suspen-domes Q4010121806b, Q6007102008d exhibit less plastic deformation as well as rather smaller displacements and exhibited collapse in a more abrupt manner, which shows that they are more prone to dynamic instability. In general, different suspen-domes subjected to the same harmonic action present two main types of failure modes, a dynamic strength failure and dynamic instability. However, it is sometimes difficult to distinguish between the two types of failure because the demarcation between the two categories is not always clear.

3.2 Responses of suspen-domes subjected to seismic action

Table 4 Structural responses of different suspen-domes subjected to different earthquakes

Label of suspen-domes	Load	Yield load* (m/s^2)	Failure load* (m/s^2)	Characteristic responses			
				D (m)	SMDE ($\times 10^6$ J)	R_{1P} (%)	R_{8P} (%)
Q4007101506a	Taft	15.50	38.00	0.14	10.25	36.34	7.60
Q4007101506a	El-Centro	16.30	44.50	0.19	0.80	66.08	5.56
Q4007101506a	Northridge	23.00	72.50	0.18	1.07	78.07	4.09
Q4007101506a	AW	12.00	79.50	0.33	7.99	81.87	40.94
Q4008101506a	Taft	20.00	37.50	0.14	8.61	38.56	6.25
Q4007121506a	Taft	15.75	29.00	0.12	5.20	32.26	4.82
Q6007082008d	Taft	23.00	39.50	0.19	3.02	32.93	4.21
Q6007102008d	Taft	18.00	33.00	0.18	3.40	24.50	3.33
Q6008082008f	Taft	24.00	41.50	0.20	7.52	34.82	8.33

* Peak Ground Acceleration (m/s^2)

Earthquake motion can be regarded as a combination of many simple harmonic waves with different frequencies and amplitudes. Therefore, it is of interest to study the responses of suspen-domes subjected to several earthquakes. Here, four ground motions including Taft (1952, Taft Lincoln School, N21°E), El-Centro (1940, El Centro Site, NS), Northridge (1994, Newhall –W Pico Canyon, N46°W) and an artificial wave (AW) are considered in order to demonstrate the difference in structural responses and failure characteristics. The normalized acceleration response spectra (*Sa*, damping ratio h=2%) corresponding to periods of these four excitations are shown in Fig. 7.

Taking the suspen-dome Q4007101506a subjected to the Taft wave for example, the responses are given in Fig. 8. Other cases for various suspen-domes as well as for different earthquake motions with several values of A were investigated in the same way as the aforementioned, and the results are listed in Table 4.

As shown in Fig. 8(a), the structural yield point appears when the peak ground acceleration A increase to 15.50 m/s^2; and the whole cross section begins to yield at A=26.00 m/s^2. The next important characteristic is that the R_{nP} and the displacements (shown in Fig. 8(b)) show sharp increases as well as the SMDE (shown in Fig. 8(c)) after experiencing almost linearly increases with increases in peak ground acceleration. Subsequently, the suspen-dome loses normal working ability as severe plastic deformation and large displacements occur, indicating a vulnerability to dynamic strength failure. The failure ground acceleration was judged to be 38.00 m/s^2, the corresponding contour of displacements is shown in Fig. 8(d). From Fig. 8(d), it can easily be found that the most severe deformation also appears in the lower part of the structure.

From Table 4, it can be seen that the plastic deformation (in columns 7 and 8) of the selected suspen-domes is becoming critical as well as the displacement (in column 5) corresponding to the failure load (in column 4), which indicates that these cases are inclined to dynamic strength failure. In addition there is a significant difference between the yield load and the failure load, meaning the suspen-domes have relatively good ability to undergo ductility and energy dissipation. Moreover, the structural responses for the same suspen-dome subjected to different seismic waves are different, such as the Q4007101506a under the action of the Taft wave, El-Centro wave, Northridge wave and AW wave. Also, there are large differences in the responses among various suspen-domes subjected to the same seismic ground motion.

4. The criterion for judging the failure load

4.1 The value, I_d, being the sum of the SED values

The structural total strain energy can be divided into elastic strain energy and plastic strain energy. Referring to single-layer spherical reticulated shells (Zhang *et al*. 2017), the SED value I_i of the ith element and the I_d (which is the sum of the I_i for all the elements) of suspen-domes can be expressed respectively in Eqs. (1) and (2)

$$I_i = \frac{1}{2}\sum_{j=1}^{n}\left(\left((\boldsymbol{\sigma}_{ij})^{\mathrm{e}}\right)^T(\boldsymbol{\varepsilon}_{ij})^{\mathrm{e}} + \left((\boldsymbol{\sigma}_{ij})^{\mathrm{p}}\right)^T(\boldsymbol{\varepsilon}_{ij})^{\mathrm{p}}\right) \tag{1}$$

where $(\boldsymbol{\sigma}_{ij})^{\mathrm{e}}$ and $(\boldsymbol{\sigma}_{ij})^{\mathrm{p}}$ are the elastic and plastic stress of the ith element to the jth integration point, respectively; $(\varepsilon_{ij})^{\mathrm{e}}$ and $(\varepsilon_{ij})^{\mathrm{p}}$ are, corresponding to $(\boldsymbol{\sigma}_{ij})^{\mathrm{e}}$ and$(\boldsymbol{\sigma}_{ij})^{\mathrm{p}}$, the elastic and plastic strain. Then, the sum of I_i, I_d, is given by Eq. (2)

$$I_d = \sum_{i=1}^{N}\sqrt{2I_i} \tag{2}$$

where N is the number of structural elements and $\sqrt{2I_i}$ is the SED value of the ith element. The I_i including both elastic and plastic strain energy is taken at the end of the time history for a given ground motion input due to the fact that plastic strain energy accumulates throughout the time history of the ground motion.

Here, the new parameter, I_d, is a function of the stress and strain, so it not only reflects their amplitudes but also implies their directions. Importantly, the I_d, represents the global structural working state because I_d as a scalar quantity is the sum of SED values for all the structural elements. Thus, a model emerges to analyze the seismic behavior of global suspen-dome through the relationship between I_d and A. The next section will show that the general characteristic point generally exists in the I_d-A relationships for suspen-domes based on the nonlinear time-history response analysis.

4.2 The criterion

As mentioned above, the I_d values including the elastic and plastic strain energy are calculated according to Eq. (2). It should be noted that the I_d is selected at the end of the time history for a given ground motion input due to the fact that plastic strain energy accumulates throughout the time history of the ground motion. Taking the suspen-dome Q4007101506a subjected to the Taft wave for example, to show the failure criterion, the I_d-A relationship is plotted as shown in Fig. 9.

It can be seen from Fig. 9, that a significant characteristic point F emerges after yield load Y. Before

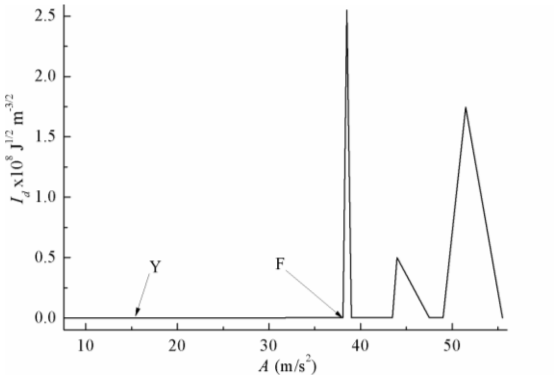

Fig. 9 The I_d-A curve of Q4007101506a subjected to the Taft wave

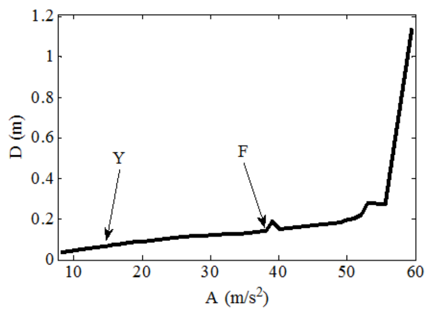

Fig. 10 The maximum nodal displacement curve of Q4007101506a subjected to the Taft wave

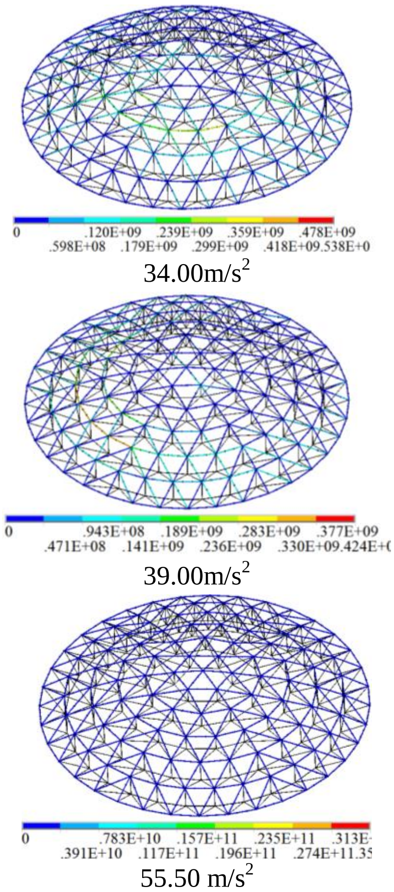

Fig. 11 The stress distribution of Q4007101506a subjected to the Taft wave

point F, the I_d almost linearly increases with the peak ground acceleration A, which means that the suspen-dome is in the normal working state; after point F, the I_d sharply increase; then, the I_d experiences a sharp fluctuation following the increasing in the peak ground acceleration until the suspen-dome collapses. Here, it is noticeable that the structure can still carry load after point F, but the structural working state is rather changeable with increasing A and rather different from the initial working state. Hence, it can be judged that the suspen-dome has lost its normal working ability after the characteristic point F has been reached.

Figs. 10 and 11 present the maximum nodal displacement curve and the stress distribution of suspen-dome Q4007101506a subjected to the Taft wave. It can be seen from Fig. 10, that the maximum nodal displacement has reached 0.186 m when the characteristic point F emerges. Actually, the maximum nodal displacement (0.186 m) to the structural span (40 m) ratio has exceeded the allowable deflection, 1/400, as recommended in the Technical Specification for Space Frame Structures (Chinese Standard 2010), which means that the suspen-dome Q4007101506a has reached its serviceability limit state.

In addition, the element stress of the suspen-dome increases with the peak ground acceleration A as shown in Fig. 11, particularly the element in the middle parts of the single-layer lattice dome. As mentioned above, when the peak ground acceleration exceeds 15.50 m/s^2, the suspen-dome begins to yield (R_{1P} is more than 0 as shown in Fig. 6(a)). Then, the structural yield level is gradually spreading throughout the member cross-sections following the increase in the peak ground motion A. When the peak ground motion A reaches 39.00 m/s^2, the yield member ratio, R_{1P}, has exceeded 50% as shown in Fig. 6(a), and the R_{8P} has reached 30%. The fully yielded members are mainly distributed in the middle parts of the single-layer lattice dome. Following a peak ground motion 39.00 m/s^2, the yield member ratio continues to increase and almost all of the elements stress has exceeded the element yield stress of 345 MPa as shown in Fig. 11.

Combining the severe plastic deformation and large displacements as shown in Fig. 8, Fig. 10 and Fig. 11, the suspen-dome is considered to have suffered dynamic strength failure after point F.

Furthermore, a failure criterion can be derived based on the point F in Fig. 9 referring to Zhang *et al*. (2017), the criterion is mathematically proposed as:

$$k_i = \frac{\left(I_{d,i} - I_{d,1}\right)\max\left(A\right)}{\left(A_i - A_1\right)\max\left(I_d\right)} \geq 1 \tag{3}$$

where k_i is the slope of the I_d-A curve between the amplitudes A_i and A_1 of the ith and 1st loads, respectively. k_i is defined as the structural failure index here.

Eq. (3) is called the SED criterion for judging the failure load (peak ground acceleration) of the suspen-domes and the corresponding load at point F is named as the failure load.

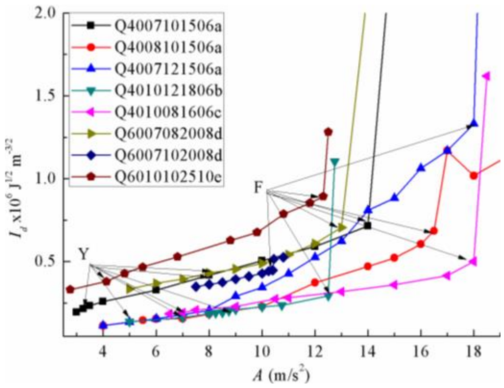

(a) Different suspen-domes subjected to 3-D harmonic wave

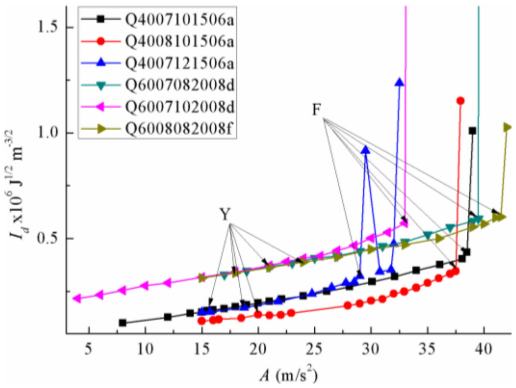

(b) Different suspen-domes subjected to Taft wave

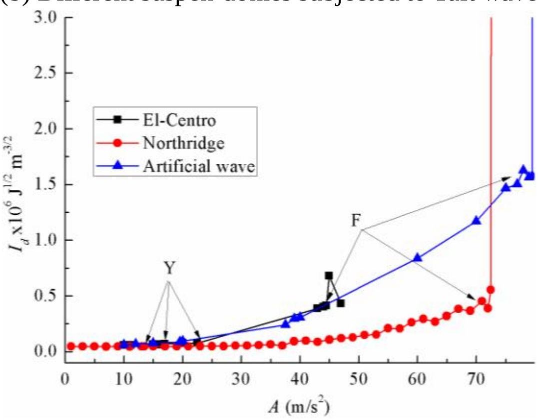

(c) Q400710156a subjected to three typical waves

Fig. 12 The I_d-A curves

4.3 The reason for the sharply increasing values of I_d

The reason why the I_d increase sharply after point F can be explained by considering membrane forces and membrane deformations both of which can store a large amount of strain energy (Cook *et al*. 2007). The strain energy (SE) of thin-walled members is given by Eq. (4)

$$SE = \frac{1}{2}\mathbf{u}_e^{\mathrm{T}}\left(\mathbf{K}_e + \mathbf{S}_e\right)\mathbf{u}_e \tag{4}$$

where $\mathbf{u}_e$ is the element displacement vector; $\mathbf{K}_e$ and $\mathbf{S}_e$ are the element bending stiffness and the element stress stiffness matrix, respectively.

The membrane forces accounted for by the element stress stiffness $\mathbf{S}_e$ act along member axes and tangent to plate and shell mid-surfaces (Cook *et al*. 2007), and the membrane force in a bar (or column) is the axial load and in a shell is the mid-surface tangent force per unit length. In a slender bar of length L, the axial stiffness ($\mathbf{S}_e = AE/L$) is much greater than bending stiffness ($\mathbf{K}_e = EI/L^3$). Similarly, in a thin-walled structure such as a shell, the membrane stiffness is typically orders of magnitude greater than the bending stiffness. Accordingly, small membrane deformations can store a large amount of strain energy, but comparatively large lateral deflections and cross-section rotations are needed to absorb this energy in bending deformations.

Before the characteristic point F, most of the elements in the suspen-dome exhibit small deformations and the corresponding membrane force in the bar or shell remains practically constant. Hence, the strain energy which mainly comes from bending deformation is relatively small. As the geometric nonlinearities, such as large displacements, large rotations and large strains, occur, the membrane force will activate and store membrane strain energy in the corresponding elements. Therefore the global structure strain energy sharply increases as shown in Fig. 9.

5. Verification of the SED criterion

In order to verify Eq. (3), the I_d values of the selected suspen-domes subjected to different ground motions are calculated based on the analytical results above. Then, the I_d-A curves from different suspen-domes subjected to a 3-D harmonic wave, the Taft wave with the suspen-dome Q4007101506a under different seismic actions are given in Fig. 12(a), (b) and (c) respectively.

It can be seen from Fig. 12 that all the I_d-A relationships have a dramatic change when the peak ground acceleration intensity increases to a certain value after the structural yield point Y, or to be more exact, the characteristic point F also exist in all the I_d-A curves for different suspen-domes under different seismic action. This fact verifies Eq. (3) to a certain extent and consequently this equation can be used to assess the structural failure loads. Also, the two key points, Y and F divide the I_d-A relationship into three parts, namely three working stages. The first stage is the state before point Y is reached. In this stage, all members in suspen-domes are in the elastic state and the relationship between I_d and A is linear. The second stage is the state from Y to F, where an increasing number of members are entering their elastic-plastic state, and the relationship between I_d and A is nonlinear. The third stage is the failure state after point F has been reached. At this stage, I_d increases rapidly with a small increment in A, and then I_d undergoes considerable fluctuation with increasing values of A. Therefore, it can be considered at this last stage that the suspen-domes have lost their stable load-bearing capacity.

6. The unity of the SED criterion

The failure modes of shell structures can be generally divided into two kinds of collapse modes, namely, dynamic strength failure and dynamic instability (Zhi *et al*. 2007) as

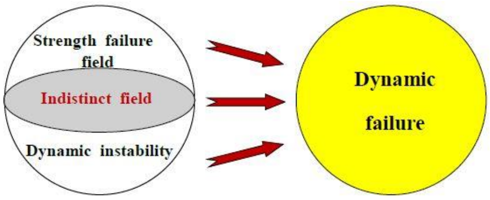

Fig. 13 The unity of the strength failure and the dynamic instability

shown in Fig. 13. Hence, two independent criteria are required to judge their corresponding failure loads, which is quite inconvenient for users. However, a particular failure mode lying in the indistinct field has now become a possibility, that is, with this specific failure mode it is difficult to distinguish a dynamic strength failure from a dynamic instability failure. For example, the failure mode of suspen-dome Q6007082008d under the action of the 3-D harmonic wave cannot be clearly distinguished. Worse still, there is no criterion to predict the failure load for the indistinct failure mode so far.

This unclear classification for the failure modes described above seriously limits the application of the failure criterion in engineering practice. Fortunately, these ambiguous classifications can be unified by the dynamic failure by use of the characteristic point F as shown in Fig. 13, and the failure loads of all the suspen-domes can be estimated by the unified SED criterion. Hence, the unified SED criterion not only simplifies the calculation of the critical load but also promotes the development of both the theory and practice in the analysis and design of suspen-domes.

7. Application of the SED-based criterion

The existing code for suspen-domes subjected to severe seismic action is heavily based on an empirical judgment of structural failure (Chen *et al*. 2010, Guo 2011). Thus, the empirical-based design code has to pay a high economic price to obtain a safe design for large-span spatial structures. Therefore, there has been extensive research efforts in the field of structural engineering to pursue a

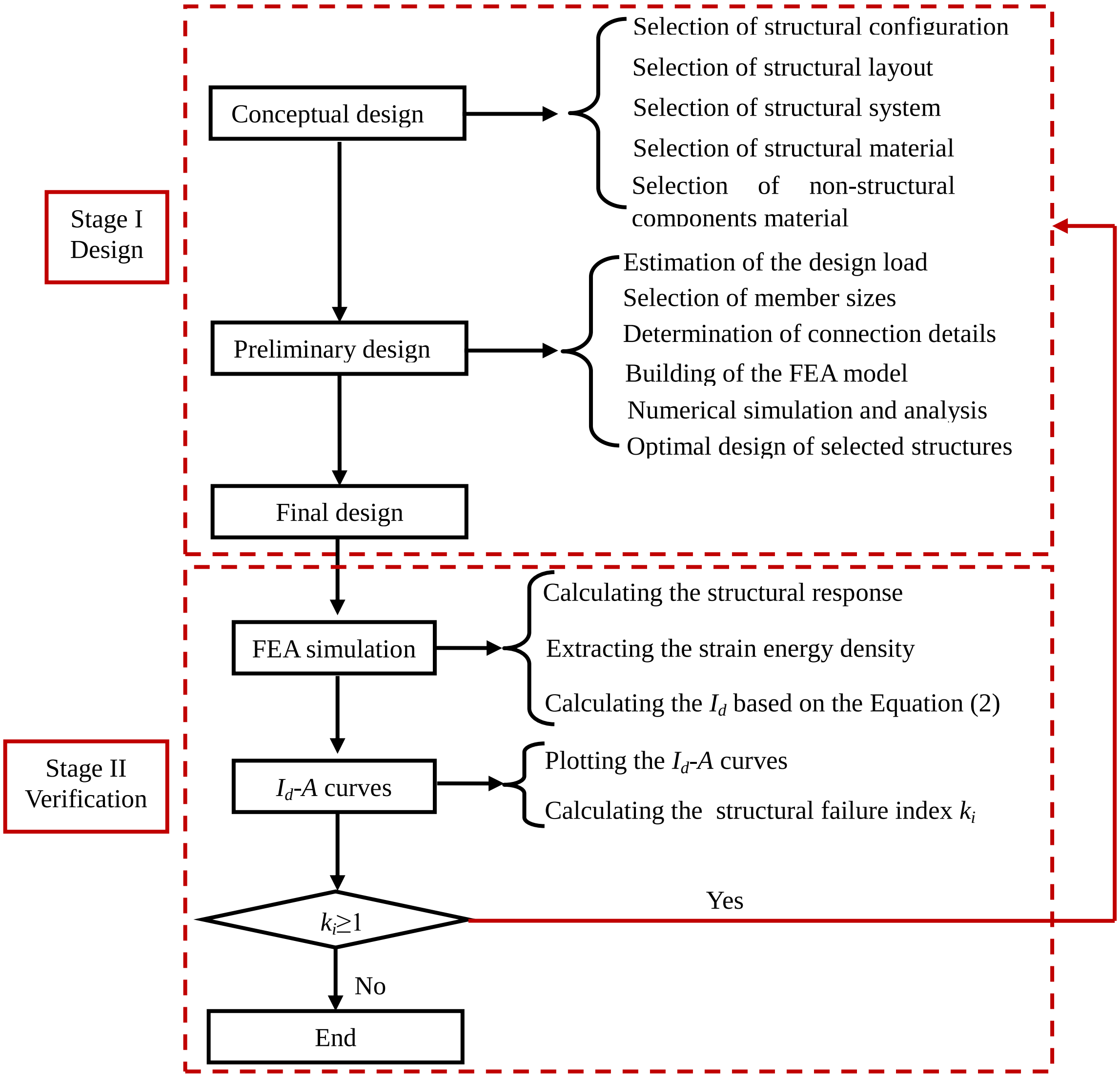

Fig. 14 The design process for suspen domes based on the SED criterion

logical-based criterion for structural anti-seismic design. The SED-based criterion provides a relatively mechanistic based method for improving the existing design code. Referring to the Chinese design code (Chinese Standard 2010) and Zhang *et al*. (2017), the design flowchart for suspen-domes using the SED-based criterion is given in Fig. 14.

The design flowchart includes two stages:

Stage I consists of two sub-sections namely conceptual design and preliminary design. The conceptual design is to select the structural type and configuration, material, the non-structural components, constraints, aesthetic expression, etc. The preliminary design is mainly to build the structural model and to set both loading case and design load values.

Stage II consists of the FEA simulation of the structural model built in Stage I, I_d-A curves and the determination of the failure load. The general FEA program is used to calculate the response of the suspen-domes under seismic load; simultaneously, the SED values of all the elements are extracted as the database for the SED-based criterion. Then, the relationship between I_d and the seismic load is investigated and the structural failure index k_i is calculated using Eq. (3). Finally, if the difference between the load value corresponding to k_i and the design load value from the design code is within the allowable limits the design process is finished, that is, the design scheme can satisfy the requirements of the design code. If this is not the case the structural configuration needs to be modified until the load value corresponding to k_i meets the design load value.

9. Conclusions

The SED model explores a new way to analyze the seismic behavior of suspen-domes based on the SED values extracted from the nonlinear time-history response analysis. The model is expected to be applicable for dynamic analyses of various types of structures. Additionally, the SED model could be used to further study data from numerical simulations and experimental tests.

Characteristic points generally existing in structural behavior are revealed through the new structural model, I_d-A relationship, and thus it is expected that the proposed criterion could be applied within the existing seismic provisions of the design code.

Significantly, the model of I_d-A can unify the two failure modes of dynamic instability and dynamic strength failure into a unified failure mode, a dynamic failure, through the characteristic point U on the I_d-A curve.

In addition, the most severe deformation for all suspen-domes as well as different earthquake motions generally appears in the lower part of the structure obtained by checking the contour of displacement of the failure state. Also for suspen-domes subjected to harmonic waves, both failure modes of dynamic instability and dynamic strength failure may appear, which are closely related to the resonant zones of the structural frequencies. For earthquake motions, suspen-domes are prone to one failure mode namely, a dynamic strength failure.

Acknowledgements

The present work has been conducted with the financial support from the National Natural Science Foundation of China (Grant No. 51608452, 51508472). The authors also thank the financial support from IEC\NSFC\170451-International Exchanges 2017 Cost Share (China) (supported by the Royal Society), China Postdoctoral Science Foundation (Grant No. 2017M621594) and the Chinese Universities Scientific Fund under Grant Nos. 10101B10096040. Special thanks to all the staffs in Space Structure Research Center of Harbin Institute of Technology for their valuable suggestions and help. In addition, the authors thank the anonymous reviewers and the Editors for their constructive comments and advice that helped greatly in improving the quality of this manuscript.

References

ANSYS 10.0. (2005), Theory Reference, ANSYS Inc..

Chen, Y. and Feng J. (2015), “Group-theoretic method for efficient buckling analysis of prestressed space structures”, *Acta. Mech.*, **226**(3), 957-973.

Chen, Z., Qiao, W. and Wang, X. (2010), “Seismic response analysis of long-span suspen-dome under multi-support excitations”, *Trans. Tianjin Univ.*, **16**, 424-432.

Chen, Z.H., Liu, H.B., Wang, X.D. and Zhou, T. (2011), “Establishment and application of cable-sliding criterion equation”, *Adv. Steel Constr.*, **7**(2), 131-143.

Chen, Z.H., Wu, Y.J., Yin, Y. and Shan, C. (2010), “Formulation and application of multi-node sliding cable element for the analysis of Suspen-Dome structures”, *Finite Elem Anal Des.*, **46**(9), 743-750.

Chen, Z.H., Wu, Y.J., Yin, Y. and Shan, C. (2010), “Formulation and application of multi-node sliding cable element for the analysis of Suspen-Dome structures”, *Finite Elem. Anal. Des.*, **46**(9), 743-750.

Chen, Z.H., Xu, H., Zhao, Z.W., Yan, X.Y. and Zhao, B.Z. (2016), “Investigations on the mechanical behavior of suspen-dome with semi-rigid joints”, *J. Constr. Steel. Res.*, **122**, 14-24.

Chen, Z.H., Yan, R.Z., Wang, X.D., Liu, H.B. and Xiao, X. (2015), “Experimental researches of a suspen-dome structure with rolling cable-strut joints”, *Adv. Steel Constr.*, **11**(1), 15-38.

Chen, Z.H., Zhao, Z.W., Zhu, H., Wang, X.D. and Yan, X.Y. (2015), “The step-by-step model technology considering nonlinear effect used for construction simulation analysis”, *Int. J. Steel Struct.*, **15**(2), 271-284.

Chinese Standard (2010), Technical Specification for Space Frame Structures, JGJ 7-2010, Beijing, China. (in China)

Cook, R.D., Malkus, D.S., Plesha, M.E. and Witt, R.J. (2007), *Concepts and Applications of Finite Element Analysis*, John Wiley & Sons, New York, NY, USA.

Gao, B.Q. and Weng, E.H. (2004), “Sensitivity analysis of cables to suspen-dome structural system”, *J. Zhejiang Univ. Sci.*, **5**(9), 1045-1052.

Guo, J.M. (2011), “Research on distribution and magnitude of initial geometrical imperfection affecting stability of suspen-dome”, *Adv. Steel Constr.*, **7**(4), 344-358.

Guo, J.M., Dong, S.L. and Yuan, X.F. (2012), “Research on static property of suspen-dome structure under heap load”, *Adv. Steel Constr.*, **8**(2), 137-152.

Kang, W.J., Chen, Z.H., Lam, H.F. and Zuo, C.R. (2003), “Analysis and design of the general and outmost-ring stiffened suspen-dome structures”, *Eng. Struct.*, **25**(13), 1685-1695.

Kitipornchai, K., Kang, W.J., Lam, H.F. and Albermani, F. (2005), "Factors affecting the design and construction of lamella suspen-dome systems", *J. Constr. Steel Res.*, **61**(6), 764-785.

Li, Q.S. and Chen, J.M. (2003), "Nonlinear elasto plastic dynamic analysis of single-layer reticulated shells subjected to earthquake excitation", *Comput. Struct.*, **81**(4), 177-188.

Li, Z.Q., Zhang, Z.H., Dong, S.L. and Fu, X.Y. (2012), "Construction sequence simulation of a practical suspen-dome in jinan olympic center", *Adv. Steel Constr*., **8**(1), 38-53.

Liu, H.B. and Chen, Z.H. (2012), "Influence of cable sliding on the stability of suspen-dome with stacked arches structures", *Adv. Steel Constr.*, **8**(1), 54-70.

Liu, X., Zhang, A., Zhang, X. and Chen, T. (2016), "Particle swarm optimization algorithm for suspen-dome structure under multiple loading cases", *Eng. Comput.*, **33**(3), 1-13.

Shen, S.Z. and Zhi, X.D. (2005), "Failure mechanism of reticular shells subjected to dynamic actions", *China Civil Eng. J.*, **38**(1), 11-20. (in Chinese)

Zhang, M., Zhou, G.C., Huang, Y.X., Zhi, X.D. and Zhang, D.Y. (2017), "An ESED method for investigating seismic behavior of single-layer spherical reticulated shells", *Earthq. Struct*., **13**(5), 455-464.

Zhang, Z.H. and Dong, S.L. (2011), "Structural design of a practical large-span cable-frame type of suspended single-layer reticulated shell with free surface", *Adv. Steel Constr.*, **7**(4), 359-375.

Zhang, Z.H., Dong, S.L. and Fu, X.Y. (2009), "Structural design of lotus arena: a large-span suspen-dome roof", *Int. J. Space Struct.*, **24**(3), 129-142.

Zhi, X.D., Fan, F. and Shen, S.Z. (2007), "Failure mechanisms of single-layer reticulated domes subjected to earthquakes", *J. IASS*., **48**(1), 29-44.

Zhi, X.D., Fan, F. and Shen, S.Z. (2010), "Elasto-plastic instability of single-layer reticulated shells under dynamic actions", *Thin Wall. Struct.*, **48**(10), 837-845.

Zhi, X.D., Fan, F. and Shen, S.Z. (2010), "Elasto-plastic instability of single-layer reticulated shells under dynamic actions", *Thin Wall. Struct.*, **48**(48), 837-845.

Zhou, Z., Wu, J. and Meng, S.P. (2014), "Influence of member geometric imperfection on geometrically nonlinear buckling and seismic performance of suspen-dome structures", *Int. J. Struct. Stab. Dyn*., **14**(3), 1-20.

CC